RSC Advances

PAPER

View Article Online
View Journal | View Issue

Cite this: *RSC Adv.*, 2025, **15**, 37216

Exploring weak noncovalent interactions in a few halo-substituted quinolones

Satyanand Kumar, [ab] Ravi Kumar, [a] Rakesh K. Mishra *[a] and Satish Kumar Awasthi *[a]

Crystal engineering utilizing weak interactions provides a real solution to increase the potential of active pharmaceutical ingredients (APIs). Quinolone derivatives represent one of the most widely used molecules, having potential applications in medical fields as antibacterials and antimalarials. This study addresses a few systematically designed and crystallographically characterized chloro- and fluoroquinolones in order to investigate the weak interactions leading to the formation of supramolecular assemblies. The interactions in crystal packing are discussed in terms of N–H···X, C–H···X (X = F, Cl), π···π, C–H···π, and lone pair (lp)···π interactions, along with unique homo- and hetero-halogen bonding, *viz.* F···F, F···Cl, Cl···O, and C–F···π, as well as C–H···H–C interactions. *N*-Ethyl derivatives exhibited the co-crystallization of solvent molecules, *viz.*, water and chloroform, creating unique supramolecular structures. Fingerprint plots generated directly from the Hirshfeld surface further supported the noncovalent interactions. The DFT studies also supported the importance of weak interactions in crystal packing. This report shows how merely switching different alkyl groups may lead to various supramolecular transformations that are valuable for designing crystals, particularly quinolone-based active pharmaceutical ingredients.

Received 22nd May 2025
Accepted 9th September 2025

DOI: 10.1039/d5ra03605d

rsc.li/rsc-advances

Introduction

The arrangement of molecules, particularly solid-state active pharmaceutical ingredients (APIs) in a crystal, determines their physicochemical properties and thus their efficiency.[1,2] In this context, the crystal engineering concept has recently become a popular tool for solving real-world problems by designing new functional drug molecules with diverse functional groups and drug delivery applications.[3,4] Among the different classes of clinical drug molecules, the quinolones represent one of the most successful classes of synthetic antibiotics. Since the introduction of nalidixic acid, the first quinolone, in 1962, structural alterations have led to the synthesis of second-, third-, and fourth-generation haloquinolones with improved activity, particularly against Gram-positive organisms.[5] Moreover, among the haloquinolones, fluoroquinolones play a part in post-exposure prophylaxis and chemotherapy for specific agents that can be used in biological warfare.[5c] Several fluoroquinolone analogs have been used to cure anthrax, cholera, plague, brucellosis, tularemia, and other infections. Surprisingly, despite their long history and novel bioactivity, to the best of our knowledge, no systematic crystallographic studies have been reported so far for quinolone analogues.

Literature surveys have revealed that hydrogen bonding,[6] *viz.* X–H···Y–Z (where X, Y are electronegative species), along with several weak interactions such as C–H···π, X···X, X···Y (X = Cl, Br, I; Y = N, O, F),[7] π···π, and lone-pair (lp)···π, play pivotal roles in the packing of molecules as well as molecular recognition in biological systems.[8] Among many other elements, halogens play various crucial roles in natural systems. Halogen substitution is generally introduced to improve membrane permeability and extend the drug's half-life;[9] therefore, many clinically used drugs are halogen-substituted.[10] These halo-compounds show unique properties in terms of highly directional non-covalent inter-halogen contacts, known as halogen bonding (XB) interactions,[11–13] which have been known to play important roles in biological systems,[14] drug design,[15] crystal engineering,[16] nonlinear optical (NLO) materials,[17] organic semiconductors,[18] magnetic materials,[19] molecular recognition,[20] molecular machines,[20a] supramolecular gels,[21] as well as in triggering phosphorescence in organic molecules,[22] which is a significant application in organic optoelectronics.

Halogen bonding is an interesting donor–acceptor type interaction involving an atom possessing one or more lone pairs of electrons (such as O, N, or S, donating electrons, functioning as a Lewis base), and a halogen atom (Cl, Br, or I functioning as a Lewis acid, accepting the lone pair of electrons). Based on interactive geometrical angles (∠C–X···X, θ_1 and θ_2), halogen

[a]*Department of Chemistry, University of Delhi, Delhi-110007, India. E-mail: satishpna@gmail.com*

[b]*Department of Chemistry, Rajdhani College, University of Delhi, Mahatma Gandhi Marg, Raja Garden, New Delhi-110015, India*

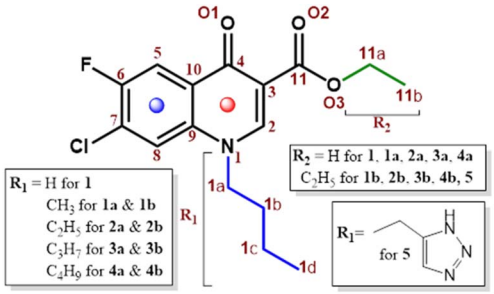

Scheme 1 Structures of the –F, –Cl substituted quinolone compounds under study, with the numbering system used for discussion.

bonds can be categorized as type I ($\theta_1 \approx \theta_2$) or type II ($\theta_1 \approx 90°$ and $\theta_2 \approx 180°$) interactions.[23] Homo-halogen interactions of both types I and II are predominant, whereas most of the X···X hetero-halogen interactions are of the type II geometry and are highly directional in nature. The halogenated compounds also possess the tendency to form a C–X···π bonding synthon between the adjacent halo phenyl rings.[24] The hierarchy of these interactions can be modified by adjusting the strength of halogen bonds by utilizing different substituents in various positions. If more than one type of non-covalent interaction is formed between the synthons, there may be cooperation,[25] or competition[26] among them.

In continuation of our past and present efforts towards understanding the chemistry of some bioactive quinolone derivatives,[27] herein, we report a detailed crystallographic study of some systematically designed chloro-/fluoroquinolones. The aim of this study is the design and synthesis of quinolone crystals, as well as their supramolecular assembly in particular arrangements by exploiting the directional intermolecular interactions as the basic tools. Herein, instead of changing the position and type of halogen atoms, we have explored the possibility of modulating the interactions only by simple alkyl substitution over the quinolone ring (Scheme 1). The substitution has led to multiple intermolecular weak interactions like classical/non-classical H-bonding (C–Cl···H, C–F···H–C, C–O···H, and C–N···H–C), halogen bonding, as well as π···π interactions, *etc.* These interactions are structurally different from each other and have different active sites for growth, thus showing various supramolecular packing patterns.

Results and discussion

The important crystallographic data for all the compounds are shown in Tables 1 (**A**, **1**–**2b**) and 2 (**2c**–**5**). The crystals of the precursor compound **A** were obtained by dissolving 10 mg of the compound in a solvent mixture of chloroform/hexane (1 : 1, v/v) at room temperature, and after a few days, transparent needle-shaped single crystals were obtained, suitable for X-ray analysis. Compound **A** crystallizes in the monoclinic $P2_1/c$ space group. The phenyl ring is found to be sandwiched between a lone pair from nitrogen and the fluorine atom, and is almost linear ($\angle NC_pF = 178.56°$) leading to interesting intermolecular interactions in terms of weak C–F···π ($dC_p\cdots F = 3.345$ Å) and lone-pair, N(lp)···π ($dC_p\cdots N = 3.354$ Å) interactions, with an intermolecular layer slipping angle of 50.21°, resembling a ladder-like motif (Fig. 1a). Probably, the strong electronegativity of fluorine gives rise to $C^{\delta+}$–$F^{\delta-}$ bond dipoles in the phenyl ring, which render the centre of the phenyl ring electropositive. The aforementioned interactions are found to be useful in efficient catalytic orientations and play various important roles in biomolecules.[28] The unsubstituted derivative of the parent compound, **1**, was obtained in the monoclinic $P2_1/n$ space group and showed Cl···O (d = 2.894 Å; 171.81°) halogen

Table 1 Crystallographic data for compounds **A**–**2b**

Compound reference	**A**	**1**	**1a**	**1b**	**2a**[27c]	**2b**
Formula	$C_{14}H_{15}ClFNO_4$	$C_{10}H_5ClFNO_3$	$C_{11}H_7ClFNO_3$	$C_{13}H_{11}ClFNO_3$	$C_{12}H_9ClFNO_3$	$C_{14}H_{13}ClFNO_3\cdot CHCl_3$
Formula mass	315.72	241.60	255.63	283.69	269.65	417.07
Crystal system	Monoclinic	Monoclinic	Triclinic	Monoclinic	Triclinic	Monoclinic
Space group	$P2_1/c$	$P2_1/n$	$P\bar{1}$	$P2_1/c$	$P\bar{1}$	$P2_1/n$
a/Å	4.3523(5)	6.2910(11)	7.1789(8)	11.9920(8)	7.1404(7)	7.2079(10)
b/Å	15.2232(16)	8.2326(14)	8.4907(7)	25.5932(18)	8.9074(11)	27.556(4)
c/Å	22.9957(18)	17.968(3)	9.3255(8)	8.1786(7)	9.3379(10)	9.2363(13)
α/°	90.00	90.000(14)	73.107(8)	90.00	72.150(10)	90.00
β/°	92.056(8)	90.000(14)	71.053(9)	91.831(6)	81.114(9)	92.329(12)
γ/°	90.00	97.441(14)	76.278(9)	90.00	85.545(9)	90.00
Volume/Å^3	1522.6(3)	922.8(3)	507.98(9)	2508.8(3)	558.25(11)	1833.0(4)
Z	4	4	2	8	2	4
μ/mm^{-1}	0.276	0.418	0.385	0.320	0.355	0.668
Temp/K	298(2)	293(2)	298(2)	298(2)	293(2)	298(2)
Number of reflections measured	6559	7104	7439	23557	4266	20925
Independent	4032	2152	2746	6830	3000	3592
R_{int}	0.0330	0.0598	0.0240	0.0485	0.0313	0.1722
R_1 ($I > 2\sigma(I)$)	0.0641	0.0631	0.0421	0.0818	0.0885	0.0991
w$R(F^2)$	0.1442	0.1667	0.1085	0.2054	0.2237	0.2391
R_1 (all data)	0.1140	0.1107	0.0584	0.1426	0.1451	0.2160
w$R(F^2)$	0.1752	0.2262	0.1197	0.2462	0.2432	0.2900
CCDC no.	843028	1447133	873772	894172	853691	929745

Table 2 Crystallographic data for compounds 2c–5

Compound reference	2c	3a	3b	4a	4b	5
Formula	$C_{14}H_{13}ClFNO_3 \cdot 3(H_2O)$	$C_{13}H_{11}ClFNO_3$	$C_{15}H_{15}ClFNO_3$	$C_{16}H_{17}ClFNO_3$	$C_{14}H_{13}ClFNO_3$	$C_{15}H_{11}ClFN_4O_3$
Formula mass	351.75	283.68	311.73	325.76	97.70	349.73
Crystal system	Triclinic	Triclinic	Monoclinic	Monoclinic	Triclinic	Monoclinic
Space group	$P\bar{1}$	$P\bar{1}$	$P2_1/n$	$P2_1/c$	$P\bar{1}$	$P2_1/n$
a/Å	7.8889(7)	8.2284(19)	10.4187(9)	10.2295(10)	9.0561(16)	8.8502(14)
b/Å	9.0771(9)	8.970(2)	11.4345(10)	16.2593(11)	9.0599(13)	20.148(3)
c/Å	12.3827(12)	9.4084(12)	12.6311(11)	9.9934(9)	9.3250(14)	9.0629(14)
α/°	99.027(8)	69.237(16)	90.00	90.00	69.818(14)	90.00
β/°	97.434(8)	74.254(15)	101.018(8)	113.612(11)	69.854(15)	108.764(17)
γ/°	107.192(8)	69.76(2)	90.00	90.00	71.629(15)	90.00
Volume/Å^3	821.95(14)	600.4(2)	1477.0(2)	1523.0(3)	657.2(2)	1530.2(4)
Z	2	2	4	4	2	4
μ/mm^{-1}	0.272	0.334	0.279	0.273	0.309	0.284
Temp/K	298(2)	298(2)	298(2)	298(2)	298(2)	293(2)
Number of reflections measured	11369	6177	9638	9902	5510	10764
Independent	3222	3278	4002	4094	3503	4145
R_{int}	0.0258	0.0198	0.0190	0.0283	0.0165	0.1279
R_1 ($I > 2\sigma(I)$)	0.0469	0.0516	0.0510	0.0665	0.0654	0.0896
w$R(F^2)$	0.1390	0.1423	0.1743	0.1685	0.2126	0.1878
R_1 (all data)	0.0615	0.0655	0.0629	0.0874	0.0863	0.2713
w$R(F^2)$	0.1536	0.1527	0.193	0.1836	0.2477	0.3029
CCDC no.	864291	963789	964919	929847	929723	1432074

bonding (which is less than the sum of their respective van der Waals radii),[29] as well as C⋯C interactions within the unit cell (Fig. 1b).

The *N*-methyl acid derivative, **1a**, crystallizes in the triclinic $P\bar{1}$ space group. Molecules are connected through $R_2^2(8)$ dimeric C_5–H⋯F hydrogen bonding (d = 2.590 Å; 161.54°) and Cl⋯O halogen bonding (d = 3.101 Å; 132.80°) interactions, resulting in the formation of a tetrameric network (Fig. 2a). The non-classical hydrogen bonding interaction C–H⋯O (d = 2.455 Å; 158.79°) also contributes to the present network structure. The coexisting halogen and hydrogen bonding interactions act as the driving force for this assembly. Compound **1a** showed strong face-to-face interaction ($dC_q \cdots C_q$ = 3.481 Å and 3.537 Å; C_p = centroid of phenyl ring; C_q = centroid of quinolone ring) in a head-to-tail manner (SI, Fig. S1). The crystal lattice of compound **1b** exhibited two crystallographically different molecules having two individual geometries (say **1b** and **1b**$^{\#}$) with respect to $>C_4$=O and $>C_{11}$=O in the monoclinic space group (SI, Fig. S2). Both isomers are almost orthogonal to each other, interacting through F⋯Cl contacts (Fig. 2b), a rare but interesting intermolecular hetero-halogen bond from a crystal engineering point of view.[30] Chlorine, which is relatively less electronegative and has more polarizable electron density, provided an electrophilic site, and the least polarizable fluorine acted as a nucleophile. Here, the fluorine serves as a halogen bond acceptor, showing the character of type II halogen bonding with dF⋯Cl = 2.967 Å, ∠CClF = 175.17° and ∠CFCl = 135.87°. It also showed weak C–F⋯HC_{11} interactions with d = 2.811 Å. The geometrical orientation around the C=O functional group was also reflected in the form of two different types of π⋯π interactions. The molecule having a C=O group on the same side (**1b**) shows stacked behaviour in a head-to-head form ($dC_q \cdots C_q$ = 3.391 Å), while **1b**$^{\#}$ shows slipped π⋯π stacking ($dC_p \cdots C_q$ = 3.436 Å) in a head-to-tail manner (SI, Fig. S3).

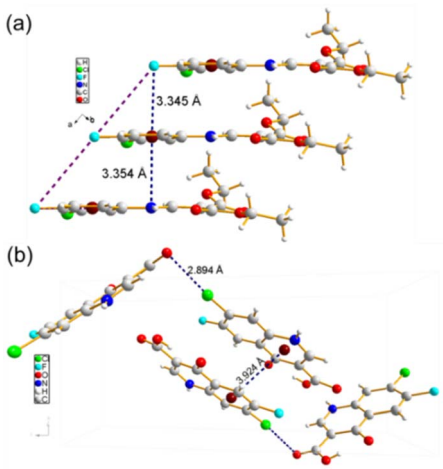

Fig. 1 (a) Ladder-like motifs formed by C–F⋯π, lp(N)⋯π contacts of **A**, and (b) Cl⋯O and π⋯π interactions in the unit cell of **1** along the *a*-axis.

The crystal of the *N*-ethyl-substituted acid derivative[27c] **2a** has been reported in a triclinic $P\bar{1}$ space group having two molecules in each unit cell. This single molecule showed both homo and hetero halogen bonding interactions: one through F⋯F, corresponding to a distribution of the type $^{\delta+}F^{\delta-} \cdots {}^{\delta+}F^{\delta-}$ (d = 2.777 Å, $\theta_1 = \theta_2$ = 154.27°, with the sum of van der Waals radii being 2.94 Å), and another side-on Cl⋯O (d = 3.099 Å; 133.43°) halogen–heteroatom interaction forming a tetrameric cluster (Fig. 3a). The π⋯π interactions ($d = C_q \cdots C_q$) were found to be 3.610 Å (SI, Fig. S4).

The crystal of **2b** was harvested from an ethyl acetate/chloroform solvent mixture, which was solved in the monoclinic $P2_1/n$ space group with a hydrogen bonding adduct of a $CHCl_3$ molecule (Fig. 3b). The host and guest components in

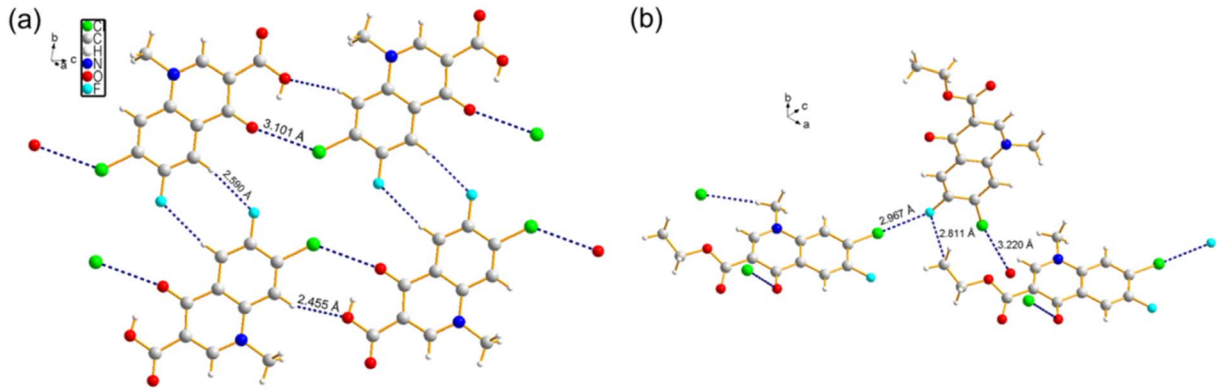

Fig. 2 (a) The front view of **1a** forming molecular sheet symmetry codes: $x, y, -1+z$; $-x, 1-y, -z$, and (b) showing the F⋯Cl, symmetry code: $1+x, y, 1+z$, as well as C–F⋯H interactions between **1b** and **1b**$^{\#}$.

the adduct are linked by $R_1^2(6)$ hydrogen bonding through $O_1\cdots H_{CHCl_3}$ (d = 2.313 Å; 124.14°) and $O_3\cdots H_{CHCl_3}$ (d = 2.412 Å; 163.67°). The **2b** molecule also showed homo halogen bonding interaction in terms of F⋯F contacts (d = 2.848 Å, $\theta_1 = \theta_2$ = 161.97°). Stacked π–π interactions were observed with $dC_p\cdots C_q$ = 3.570 Å and $C_q\cdots C_q$ = 3.590 (SI, Fig. S5).

The above observation motivated us to get the crystal of **2c** in different solvent mixtures, and by slow evaporation of a solvent mixture of ethyl acetate/ethanol, it was found to crystallize in the triclinic $P\bar{1}$ space group along with three guest molecules of water interacting *via* hydrogen bonding (Fig. 3c, top). All three water molecules are interconnected by $R_4^4(8)$ hydrogen bonding in two different rectangular planes of interactions (Fig. 3c, bottom). The angles between the two rectangular planes of water molecules are approximately 139.29° and 122.27°, with O–H⋯O bond distances in range of 1.927–2.193 Å, while the bond angles ∠OHO range from 151.46–170.28° ($\angle O_{1s}HO_{2s}$ = 167.84°, $\angle O_{2s}HO_{1s}$ = 170.28°, $\angle O_{3s}HO_{2s}$ = 162.72°, $\angle O_{2s}HO_{3s}$ = 162.79°, $\angle O_{1s}HO_4$ = 156.56°, $\angle O_{3s}HO_4$ = 151.46°).

A three-dimensional structure was constructed around the water molecules *via* the $R_4^2(8)$ hydrogen bonding network stabilizing the molecule (Fig. 3d). The guest molecules act as the

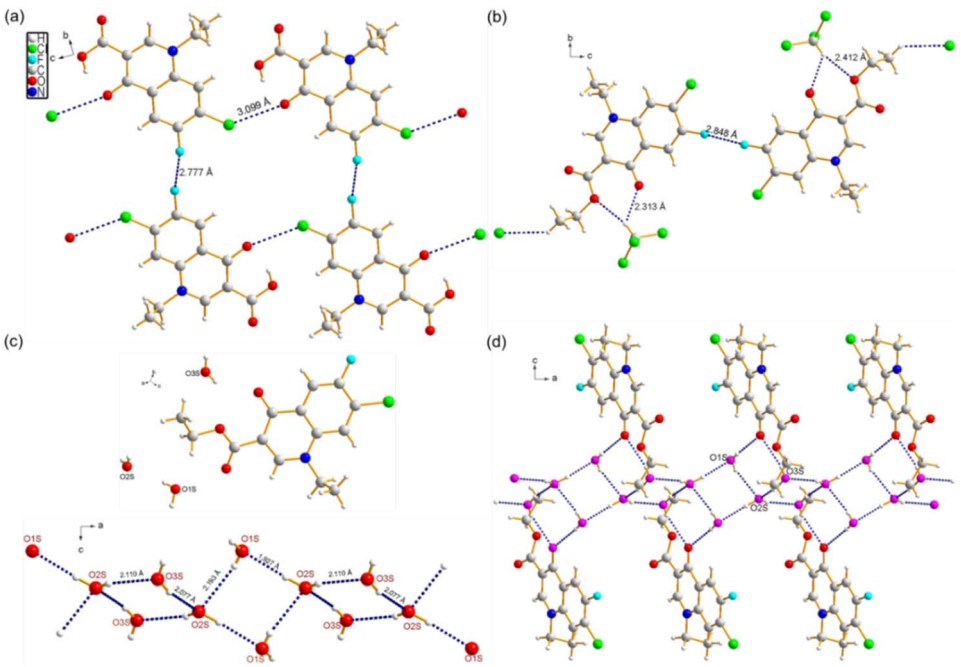

Fig. 3 (a) Tetrameric synthons of **2a** through halogen bonding (F⋯F, Cl⋯O) interactions, along the *a*-axis. (b) Crystal structure of **2c** with chloroform connected through hydrogen bonding and intermolecular homo halogen (F⋯F) bonding interactions, along the *a*-axis. (c) Crystal of **2b** with co-crystalized water molecules (up) and $R_4^4(8)$ hydrogen bonding interaction patterns among the three water molecules in two different planes (down). (d) View of the **2b** along the *b*-axis having three water molecules in crystal packing forming a channel through the $R_4^2(8)$ H-bonds to form 3-D supramolecular structures (colours of oxygen atoms of water molecules have been kept pink in order to discriminate from other oxygen atoms).

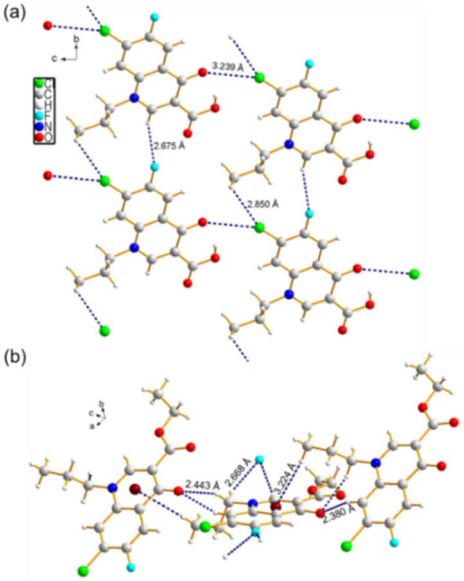

Fig. 4 (a) Compound **3a**, showing a tetramer structure formed by hydrogen and halogen bonding contacts. (b) Compound **3b**, comprising C–H···π, C–H···F, and C–H···O interactions.

backbone of the cyclic structure through hydrogen bonding, along with the Cl···H (d = 2.937 Å; 133.19°) interactions (SI, Fig. S6a and b). These types of interactions are well known for playing a key role in the stabilization of co-crystals of active pharmaceutical ingredients.[31] The same showed stacked π–π interactions with dCp···Cq = 3.537 and dCp···Cp = 3.652 Å (SI, Fig. S6c).

The *N*-propyl-substituted acid **3a** was found to have a triclinic crystal system with a $P\bar{1}$ space group forming a tetrameric structure through C_2–H···F, unsymmetrical Cl···O halogen bonding (d = 3.001 Å; 132.39), and C_{1c}–H···Cl hydrogen bonding (d = 2.850; 120.65), where Cl is coordinated to one of the hydrogen atoms of the methyl group (Fig. 4a). Molecules are stacked through slipped π···π and C···C interactions with $dC_q \cdots C_q$ = 3.612 Å and $dC_7 \cdots C_5$ = 3.350 Å (SI, Fig. S7).

The ester derivative **3b** does not show any strong π···π interactions; instead, several intermolecular C–H interactions were observed (Fig. 4b). One of the methyl hydrogens of the *N*-propyl group exhibited a significantly weak attractive electrostatic C–H···π interaction (d = 3.224; 170.96°).[32] The fluorine atom is hydrogen bonded to the two-hydrogen atoms, *i.e.*, one with C_8–H···F (d = 2.452 Å; 172.23°), while another with the hydrogen of the CH_2 group attached to the nitrogen atom (C_{1a}–H···F, d = 2.668 Å; 135.40°). The $>C_4$=O also showed hydrogen bonding in terms of C_8–H···O (d = 2.380 Å; 149.05°) and C_{1a}–H···O (d = 2.443 Å; 115.44°) interactions.

The *N*-butyl derivative **4a** crystallizes in the monoclinic $P2_1/c$ space group, which shows the presence of C1c/1d–H···Cl ((d = 2.912 Å, ∠C_{1d}HCl = 149.97°, ∠C_{1c}HCl = 117.46°), °), $R_2^2(10)$

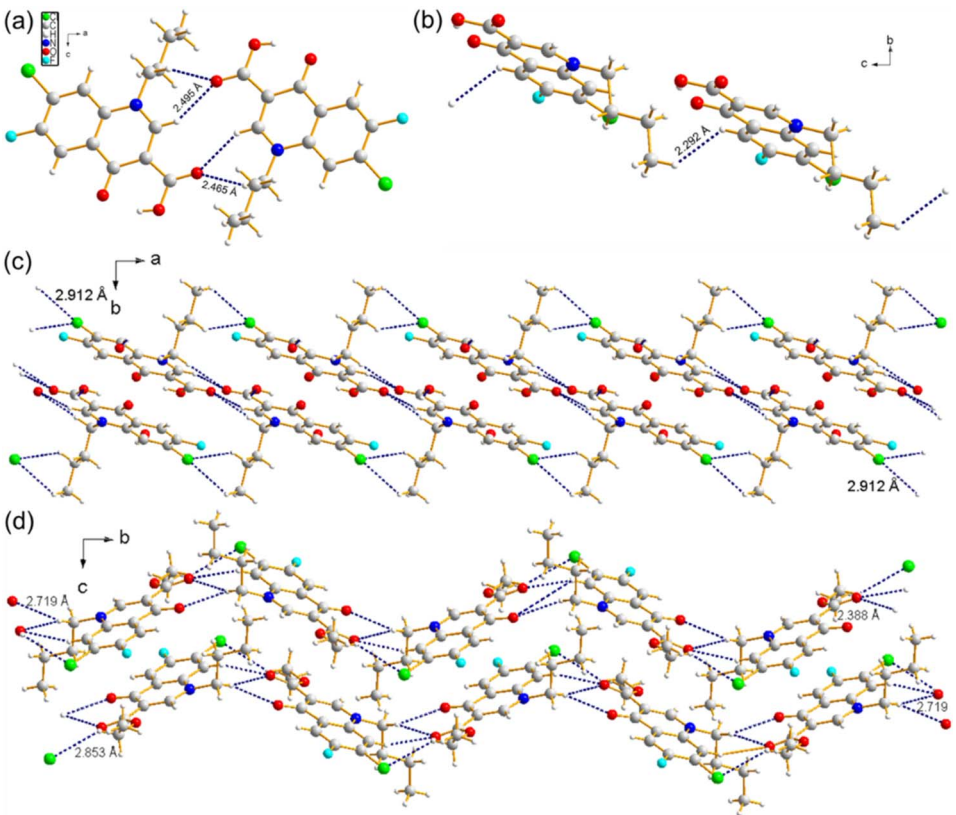

Fig. 5 (a) Front view representation of compound **4a**, showing the $R_2^2(10)$ hydrogen-bonded dimeric structure. (b) C–H···H–C interaction. (c) An extended structure along the *c*-axis formed by π···π and C–H···Cl interactions. (d) **4b**, showing a layered structure formed by hydrogen bonding and π···π interactions.

Table 3 Important halogen bonding characteristics observed

Compounds	Type of bonding	Distances (Å)	Symmetry codes
1	$Cl_1\cdots O_1$	2.894	$-1/2 + x, 1/2 - y, -1/2 + z$
1a	$O_1\cdots Cl_1$	3.101	$x, y, -1 + z$
1b	$Cl_2\cdots F_2$	2.967	$1 + x, y, 1 + z$
2a	F⋯F	2.777	$1 - x, 2 - y, -z$
	$O_1\cdots Cl$	3.099	$x, y, -1 + z$
2c	$F_1\cdots F_1$	2.848	$-x, -y, 2 - z$
3a	$O_3\cdots Cl_1$	3.239	$x, y, -1 + z$

interactions with C_2–H⋯O_{11} ($d = 2.495$ Å; 149.97°) and C_{2a}–H⋯O_4 ($d = 2.465$ Å; 158.71°), leading to a polymeric chain structure (Fig. 5a and c). Another exciting observation is the intermolecular heteropolar type C–H⋯H–C interactions between sp^3 C_{2a}–H and sp^2 C_5–H with dH⋯H = 2.292 Å (Fig. 5b), which is less than the sum of the van der Waals radius of the hydrogen atoms (2.4 Å), indicating the possibility of dihydrogen (H⋯H) bonding.[33] The molecules are stacked through π⋯π interactions with $d$$C_q$⋯$C_q$ = 3.569 Å and dCp⋯Cq = 3.584 Å (SI, Fig. S8).

On the other hand, the ester derivative **4b** was solved in the triclinic $P\bar{1}$ space group. The molecules are held together by bifurcated C–H⋯O interactions *via* C_{1a}–H⋯O_1 (d = 2.719 Å), C_{1a}–H⋯O_2 (d = 2.388 Å), C_8–H⋯O_2 (d = 2.477 Å), as well as C_{11a}–H⋯Cl (d = 2.853 Å) contacts. In the crystal lattice, strong C⋯C interactions were observed with $d$$C_{11}$⋯$C_{11}$ = 3.361 Å, along with π⋯π interactions $d$$C_p$–$C_q$ = 3.740 (SI, Fig. S9). These interactions contribute to a two-dimensional extended structure (Fig. 5d). It is noteworthy that, unlike **1a–3b**, the *n*-butyl-substituted molecules, *i.e.*, **4a** and **4b**, failed to show any tendency for C–H⋯F or halogen bonding-type interactions; it is probable that the long alkyl group restricts the molecules from coming closer from sideways.

The halogen bonding and π–π stacking interactions observed in the present work have been summarized in Tables 3 and 4, respectively.

Compound **5** differs from the other molecules, having an *N*-substituted cyclic 1-methyl triazole unit instead of a linear alkyl chain. It showed prominent C⋯H interactions in the lattice packing, while no prominent halogen bonding or C⋯C interactions were observed. The nitrogen atoms of the triazole unit displayed N⋯HC hydrogen bonding interactions with d = 2.552 Å; 152.72° and d = 2.642 Å; 145.20°. Another important interaction was observed in terms of N⋯O with d = 2.903 Å (Fig. 6).[34]

The ORTEP plots of the compounds (**1–5**) have been provided in the SI (Fig. S10).

Fingerprint plot analysis

To quantify the intermolecular noncovalent interactions as described above, the corresponding 2D fingerprint plots were generated directly from the Hirshfeld surface calculated in CrystalExplorer 21,[35] exhibiting the percentage of area occupied by various types of weak noncovalent intermolecular interactions. A few representative fingerprint plots are shown in Fig. 7. The plots show the Cl⋯O (**1**: 7.0%; **1a**: 3.4%; **2a**: 6.1%; **3a**: 5.1%), F⋯F (**2a**: 1.9%, and **2b**: 1.6%), H⋯F (**3a**: 10.6%; **3b**: 11.6%), H⋯O (**1a**: 22.8%; **3b**: 17.8%; **4a**: 23.7%; **4b**: 15.0%), Cl⋯H (**2c**: 12.2%, **3a**: 11.9%, **4b**: 12.6%), and C⋯C (**4b**: 4.9%) interactions, exhibiting the most relevant noncovalent intermolecular interactions and thus supporting the supramolecular structures formed as discussed above. The presence of C⋯C interaction in **4b** supports the strong π⋯π stacking interactions in the crystal packing.

Density functional theory (DFT) studies

To support the role of weak interactions in crystal packing, density functional theory studies were performed for a few structures. Compounds **1** and **1a** were chosen as representative examples for this purpose. The isolated monomers, corresponding crystal packing, as well as extended tetramer structures of **1** and **1a**, were optimized at the B3LYP-D4/def2-TZVP level of theory. The optimized geometries of **1** (Fig. 8a) and **1a** (Fig. 8a) monomers were quite close to the crystal structure conformation, suggesting that the monomers are in a relaxed

Table 4 π–π stacking interactions in quinolone derivatives[a]

Compounds	Angle (°)	R_1 (Å) $d$$C_p$⋯$C_q$	R_2 (Å) $d$$C_q$⋯$C_q$	D (Å) C⋯C contacts/symmetry codes
A	0.00	4.352	⋯	$C_6\cdots C_9 = 3.351\ (1 - x, 1 - y, 1 - z)$
1	0.00	3.924	3.354	$C_4\cdots C_6 = 3.361\ (1 - x, 1 - y, 1 - z)$
1a	0.00		3.481 & 3.537	$C_2\cdots C_9 = 3.395\ (1 - x, -y, -z)$
1b	4.82	3.436	4.095	$C_8\cdots C_{10} = 3.368\ (-1 - x, 1 - y, -z)$
	0.00[b]	4.060[b]	3.391[b]	$C_2\cdots C_{10} = 3.333\ (x, 1/2 - y, -1/2 + z)$
2a	0.62	⋯	3.610	$C_4\cdots C_9 = 3.323\ (x, 1 - y, -z)$
2b	0.00	3.570	3.590	$C_4\cdots C_9 = 3.328\ (1 - x, -y, 1 - z)$
2c	0.00	3.537	3.652	$C_4\cdots C_9 = 3.328\ (1 - x, -y, 1 - z)$
3a	0.00	⋯	3.612	$C_4\cdots C_9 = 3.285\ (-x, 1 - y, 1 - z)$
3b	—	⋯	⋯	⋯
4a	0.00	3.584	3.569	$C_{10}\cdots C_{10} = 3.391\ (1 - x, -y, 2 - z)$
4b	0.00	3.740	⋯	⋯

[a] R_1, R_2 = centroid–centroid distances; C_p = centroid of phenyl ring, C_q = centroid of quinolone ring, D = distance between the selected carbon atoms. [b] For **1b**#.

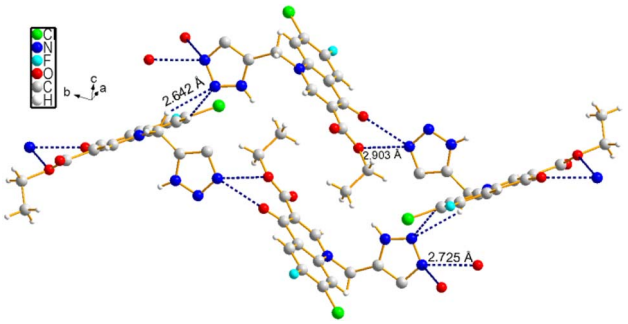

Fig. 6 Front view representation of **5** showing the tetrameric structure with the help of N···HC and N···O interactions.

conformation (SI, Table S1). The weak intermolecular interaction in the tetramer unit of **1** was computed to be −50.9 kcal mol^{-1}, while for **1a**, it was −57.9 kcal mol^{-1}. The stabilization energies were computed, including the basis set superposition error (BSSE) with a geometrical counterpoise-type correction scheme (GCP). The strong stabilization in **1a** is due to strong π···π stacking, as evident from the ring distances (3.736 and 3.663 Å) represented by dummy atoms (X), while in the case of **1**, this distance is 4.211 Å. The intermolecular Cl···O bond distances in **1** and **1a** were computed to be 2.906 and 3.322 Å, respectively, and well matched with crystal structures. The intermolecular Cl···H and N–H···O/O–H bond distances are 2.752 and 1.802 Å/2.776 Å in **1**, which are within the interaction range (Fig. 7a). Similarly, intermolecular Cl···H–O (2.969 Å) and C–H···O–H (2.189 Å) are within interaction range (Fig. 8b). Thus, strong π–π stacking, and weak halogen and hydrogen

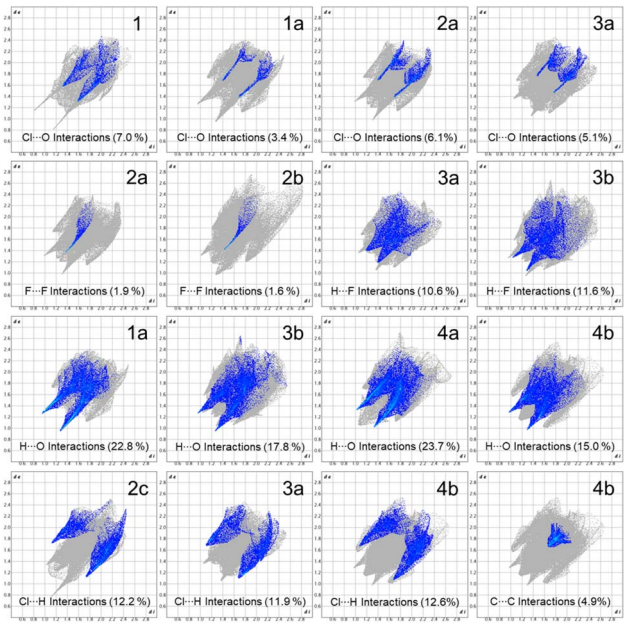

Fig. 7 The two-dimensional fingerprint plots exhibiting contributions from important weak noncovalent interactions. The inset shows the compound codes, while the percent contributions are mentioned in the individual boxes.

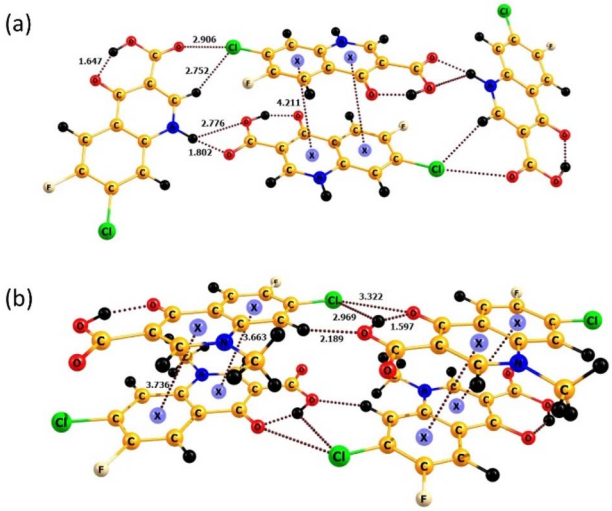

Fig. 8 B3LYP-D4/def2-TZVP-optimized tetramer structures of (a) **1** and (b) **1a**. Here, X atoms are dummy atoms and all the distances are given in Ångström (Å).

bonding intermolecular interactions are sufficient for better crystal packing.

Experimental

All chemicals used in this work were of reagent grade. They were commercially available and used as purchased without further purification. All the quinolone derivatives **A** and **1–5** in the present study have been characterized using standard spectroscopic techniques.

Synthesis of quinolones

The precursor molecule **A** and quinolone derivatives **1–5** have been synthesized by the reported method (SI, Scheme S1).[36,27a] Briefly, the condensation of 3-chloro-4-fluoroaniline with diethylethoxymethylene malonate ester at 100 °C followed by cyclization in diphenyl ether at 250 °C gave 7-chloro-6-fluoro-4-oxo-1,4-dihydroquinoline-3-carboxylic acid ethyl ester in good yield. Subsequent alkylation with several alkyl halides, utilizing either K_2CO_3 or NaH in DMF, yielded the respective *N*-alkylated products. The corresponding acid derivatives were obtained by hydrolysis of ethyl ester derivatives using a 2 N NaOH solution.

X-ray crystallography

For all twelve compounds (**A**, **1–5**), the intensity data were collected using a Bruker SMART APEX-II CCD diffractometer, equipped with a fine focus 1.75 kW sealed tube, with MoK_α radiation (λ = 0.71073 Å) at 298(2) K. Cell parameters were retrieved using APEX II software[37] and refined using SAINT on all observed reflections. Data reduction was done using SAINT software, which corrected Lorentz and polarizing effects. Scaling and absorption corrections were applied using the SADABS[38] multiscan technique. All structures were solved using SHELXS-97 (ref. 39) by direct methods and refined with full-

matrix least-squares on F^2 using the SHELXL-97 program package.[40] All non-hydrogen atoms were refined anisotropically. Structural illustrations were drawn using DIAMOND,[41] as well as ORTEP.

DFT studies

DFT studies were performed using the ORCA 6.0.1 program.[42] All the structures were optimized using the B3LYP functional and def2-TZVP basis set with D4 dispersion correction (B3LYP-D4/def2-TZVP level of theory).[43] Vibrational frequencies were computed to determine the true minima, where no negative (imaginary) frequency was present. The basis set superposition error (BSSE) utilizing the geometrical counterpoise-type correction scheme (GCP) was also computed at the same level of theory for the tetramers of **1** and **1a**.[44]

Conclusions

The present work provides a detailed, systematic, and comparatively simpler crystal engineering approach to develop a series of halo (–F/–Cl)-substituted quinolones (**1–5**), including the precursor molecule **A**. These molecules exhibited a broad range of novel weak interactions through C–H···F, C–F···π, lp···π (**A**), homo and hetero halogen bonding interactions (F···F & Cl···O in **1**, **1a**, **1b**, **2a**, **2b**, **3a**), C–H···H–C (**4a**), along with a variety of classical and non-classical hydrogen bonding contacts just by small structural modification. The co-crystallization of the solvent molecules like chloroform (**2b**) and water (**2c**), leading to beautiful 3D structures, was revealed. The 1-methyltriazole-substituted compound **5** showed N···O interactions. The nature of interactions varied with the length of the alkyl group, along with the ester or acid group. The fingerprint plot analysis provided a quantitative measurement of the weak interactions. In addition, a closer investigation of **1** and **1a** using DFT indicated intermolecular π–π stacking and other weak interactions, which contributed significantly to the stabilization of crystal packing. The present study might be helpful for addressing the challenges, design, and development of rational solid-state-active pharmaceutical ingredients (APIs) involving halo-quinolones, in terms of how well the crystal engineering can be applied towards small organic molecules, just by a simple modification.

Author contributions

Satyanand Kumar: validation, formal analysis, investigation, data curation, writing – original draft. Ravi Kumar: formal analysis, investigation, resources, writing – review & editing, Rakesh K. Mishra: methodology, software, resources, investigation, visualization, writing – review & editing, Satish Kumar Awasthi: conceptualization, resources, writing – review & editing, project administration, supervision.

Conflicts of interest

There are no conflicts to declare.

Data availability

CCDC 843028, 853691, 864291, 873772, 894172, 929723, 929745, 929847, 963789, 964919, 1432074 and 1447133 contain the supplementary crystallographic data for this paper.[45a–k]

The data supporting this article have been included as part of the supplementary information (SI). Synthetic scheme, figures exhibiting the weak interactions, ortep plots and DFT optimized coordinates. See DOI: **https://doi.org/10.1039/d5ra03605d**.

Acknowledgements

SKA is thankful to the University of Delhi for financial assistance and the University Scientific Instrumentation Centre (USIC), University of Delhi, Delhi-110007, India, for providing necessary instrumental facilities. SK is thankful to UGC, New Delhi, for financial assistance in the form of SRF.

References

1 S. Datta and D. J. W. Grant, *Nat. Rev. Drug Discovery*, 2004, **3**, 42–57.
2 M. L. Peterson, M. B. Hickey, M. J. Zaworotko and Ö. Almarsson, *J. Pharm. Pharmaceut. Sci.*, 2006, **9**, 317–326.
3 (*a*) I. D. H. Oswald, D. R. Allan, P. A. McGregor, W. D. S. Motherwell, S. Parson and C. R. Pulham, *Acta Crystallogr., Sect. B:Struct. Sci.*, 2002, **58**, 1057–1066; (*b*) J. F. Remenar, S. L. Morissette, M. L. Peterson and B. Moulton, *J. Am. Chem. Soc.*, 2003, **125**, 8456–8457; (*c*) B. R. D. Walsh, M. W. Bradner, S. Fleischman, L. A. Morales, B. Moulton, N. Rodríguez-Hornedo and M. J. Zaworotko, *Chem. Commun.*, 2003, 186–187.
4 (*a*) M. J. Daviesa, L. Setona, N. Tiernan, M. F. Murphy and P. Gibbons, *Int. J. Pharm.*, 2011, **421**, 1–11; (*b*) M. Baldrighi, G. Cavallo, M. R. Chierotti, R. Gobetto, P. Metrangolo, T. Pilati, G. Resnati and G. Terraneo, *Mol. Pharmaceutics*, 2013, **10**, 1760–1772.
5 (*a*) J. S. Wolfson and D. C. Hooper, *Antimicrob. Agents Chemother.*, 1989, **33**, 1655–1661; (*b*) D. C. Hooper, *Biochim. Biophys. Acta*, 1998, **1400**, 45–61; (*c*) P. Grohs and I. Podglajen, *Antimicrob. Agents Chemother.*, 2004, **48**, 3024–3027.
6 (*a*) G. R. Desiraju and T. Steiner in *The Weak Hydrogen Bond*, Oxford University Press, Oxford, 1999; (*b*) G. R. Desiraju, *Angew. Chem., Int. Ed.*, 2011, **50**, 52–59.
7 G. R. Desiraju, *Chem. Commun.*, 2005, 2995–3001.
8 (*a*) L. G. Volkert and M. Conrad, *J. Theor. Biol.*, 1998, **193**, 287–306; (*b*) R. Taylor, *CrystEngComm*, 2014, **16**, 6852–6865.
9 P. Zhou, F. Tian, J. Zou and Z. Shang, *Mini-Rev. Med. Chem.*, 2010, **10**, 309–314.
10 E. Parisini, P. Metrangolo, T. Pilati, G. Resnati and G. Terraneo, *Chem. Soc. Rev.*, 2011, **40**, 2267–2278.
11 (*a*) P. Metrangolo, J. S. Murray, T. Pilati, P. Politzer, G. Resnati and G. Terraneo, *Cryst. Growth Des.*, 2011, **11**, 4238–4246; (*b*) P. Metrangolo and G. Resnati, *Cryst. Growth Des.*, 2012, **12**, 5835–583; (*c*) A. Priimagi, G. Cavallo,

P. Metrangolo and G. Resnati, *Acc. Chem. Res.*, 2013, **46**, 2686–2695; (*d*) A. Mukherjee, S. Tothadi and G. R. Desiraju, *Acc. Chem. Res.*, 2014, **47**, 2514–2524; (*e*) P. Ravat, S. SeethaLekshmi, S. N. Biswas, P. Nandy and S. Varughese, *Cryst. Growth Des.*, 2015, **15**, 2389–2401.

12 (*a*) P. Auffinger, F. A. Hays, E. Westhof and P. S. Ho, *Proc. Natl. Acad. Sci. U. S. A.*, 2004, **101**, 16789–16794; (*b*) P. Metrangolo, F. Meyer, T. Pilati, G. Resnati and G. Terraneo, *Angew. Chem., Int. Ed.*, 2008, **47**, 6114–6127; (*c*) Y. Lu, T. Shi, Y. Wamg, H. Yang, X. Yan, X. Luo, H. Jiang and W. Zhu, *J. Med. Chem.*, 2009, **52**, 2854–2862.

13 A. C. Legon, *Phys. Chem. Chem. Phys.*, 2010, **12**, 7736–7747.

14 (*a*) F. T. Martins, N. Paparidis, A. C. Doriguetto and J. Ellena, *Cryst. Growth Des.*, 2009, **9**, 5283–5292; (*b*) M. R. Scholfield, C. M. V. Zanden, M. Carter and P. S. Ho, *Protein Sci.*, 2013, **22**, 139–152.

15 (*a*) D. M. Himmel, K. Das, A. D. Clark, S. H. Hughes, A. Benjahad, S. Oumouch, J. Guillemont, S. Coupa, A. Poncelet, I. Csoka, C. Meyer, K. Andries, C. H. Nguyen, D. S. Grierson and E. Arnold, *J. Med. Chem.*, 2005, **48**, 7582–7591; (*b*) Y. Lu, Y. Wang and W. Zhu, *Phys. Chem. Chem. Phys.*, 2010, **12**, 4543–4551; (*c*) S. Mahapatra, T. S. Thakur, S. Joseph, S. Varughese and G. R. Desiraju, *Cryst. Growth Des.*, 2010, **10**, 3191–3202.

16 (*a*) R. B. Walsh, C. W. Padgett, P. Metrangolo, G. Resnati, T. W. Hanks and W. T. Pennington, *Cryst. Growth Des.*, 2001, **1**, 165–175; (*b*) P. Metrangolo, G. Resnati, T. Pilati and S. Biella, *Structure and Bonding*, Springer-Verlag Berlin Heidelberg, 2008, vol. 126, pp. 105–136.

17 (*a*) S. George, A. Nangia, C.-K. Lam, T. C. W. Mak and J.-F. Nicoud, *Chem. Commun.*, 2004, 1202–1203; (*b*) E. Cariati, A. Forni, S. Biella, P. Metrangolo, F. Meyer, G. Resnati, S. Righetto, E. Tordin and R. Ugo, *Chem. Commun.*, 2007, 2590–2592.

18 M. Fourmigue and P. Batail, *Chem. Rev.*, 2004, **104**, 5379–5418.

19 G. R. Hanson, P. Jensen, J. McMurtrie, L. Rintoul and A. S. Micallef, *Chem.–Eur. J.*, 2009, **15**, 4156–4164.

20 (*a*) P. Metrangolo, H. Neukirch, T. Pilati and G. Resnati, *Acc. Chem. Res.*, 2005, **38**, 386–395; (*b*) A. Caballero, L. Swan, F. Zapata and P. D. Beer, *Angew. Chem., Int. Ed.*, 2014, **53**, 1–6.

21 L. Meazza, J. A. Foster, K. Fucke, P. Metrangolo, G. Resnati and J. W. Steed, *Nat. Chem.*, 2013, **5**, 42–47.

22 (*a*) O. Bolton, K. Lee, H.-J. Kim, K. Y. Lin and J. Lim, *Nat. Chem.*, 2011, **3**, 205–210; (*b*) J. Xu, A. Takai, Y. Kobayashi and M. Takeuchi, *Chem. Commun.*, 2013, **49**, 8447–8449; (*c*) H. Y. Gao, X. R. Zhao, H. Wang, X. Pang and W. J. Jin, *Cryst. Growth Des.*, 2012, **12**, 4377–4387.

23 (*a*) P. Metrangolo, F. Meyer, T. Pilati, G. Resnati and G. Terraneo, *Angew. Chem., Int. Ed.*, 2008, **47**, 6114–6127; (*b*) T. T. Bui, S. Dahaoui, C. Lecomte, G. R. Desiraju and E. Espinosa, *Angew. Chem., Int. Ed.*, 2009, **48**, 3838–3841; (*c*) G. Cavallo, P. Metrangolo, R. Milani, T. Pilati, A. Priimagi, G. Resnati and G. Terraneo, *Chem. Rev.*, 2016, **116**, 2478–2601.

24 C. B. Aakeröy, S. Panikkattu, P. D. Chopade and J. Desper, *CrystEngComm*, 2013, **15**, 3125–3136.

25 (*a*) S. Zhu, C. Xing, W. Xu, G. Jin and Z. Li, *Cryst. Growth Des.*, 2004, **4**, 53–56; (*b*) C. B. Aakeröy, J. Desper, B. A. Helfrich, P. Metrangolo, T. Pilati, G. Resnati and S. Andrea, *Chem. Commun.*, 2007, 4236–4238.

26 G. G. Rajulu, H. S. B. Naik, A. Viswanadhan, J. Thiruvengadam, K. Rajesh, S. Ganesh, H. Jagadheshan and P. K. Kesavan, *Chem. Pharm. Bull.*, 2014, **62**, 168–175.

27 (*a*) S. K. Dixit, N. Mishra, M. Sharma, S. Singh, A. Agarwal, S. K. Awasthi and V. K. Bhasin, *Eur. J. Med. Chem.*, 2012, **51**, 52–59; (*b*) M. K. Singh, R. Tilak, G. Nath, S. K. Awasthi and A. Agarwal, *Eur. J. Med. Chem.*, 2013, **63**, 635–644; (*c*) S. K. Dixit, N. Yadav, S. Kumar, L. Good and S. K. Awasthi, *Med. Chem. Res.*, 2014, **23**, 5237–5249.

28 (*a*) E. Kryachko and S. Scheiner, *J. Phys. Chem. A*, 2004, **108**, 2527–2535; (*b*) M. Egli and S. Sarkhel, *Acc. Chem. Res.*, 2007, **40**, 197–205; (*c*) T. J. Mooibroek, P. Gamez and J. Reedijk, *CrystEngComm*, 2008, **10**, 1501–1515; (*d*) X. Xu, B. Pooi, H. Hirao and S. H. Hong, *Angew. Chem., Int. Ed.*, 2014, **53**, 1283–1287.

29 A. Bondi, A van der Waals Volumes and Radii, *J. Phys. Chem.*, 1964, **68**, 441–451.

30 (*a*) T. Sakurai, M. Sundaralingam and G. A. Jeffrey, *Acta Crystallogr.*, 1963, **16**, 354–363; (*b*) N. Ramasubbu, R. Parthasarathy and P. Murray-Rust, *J. Am. Chem. Soc.*, 1986, **108**, 4308–4314; (*c*) G. R. Desiraju and R. Parthasarathi, *J. Am. Chem. Soc.*, 1989, **111**, 8725–8726; (*d*) B. K. Saha, A. Nangia and J. F. Nicoud, *Cryst. Growth Des.*, 2006, **6**, 1278–1281; (*e*) V. R. Hathwar and T. N. Guru Row, *J. Phys. Chem. A*, 2010, **114**, 13434–13441.

31 C. B. Aakeröy, S. Forbes and J. Desper, *CrystEngComm*, 2012, **14**, 2435–2443.

32 (*a*) M. Nishi, *CrystEngComm*, 2004, **6**, 130–158; (*b*) M. J. Plevin, D. L. Bryce and J. Bois-bouvier, *Nat. Chem.*, 2010, **2**, 466–471; (*c*) S. Karthikeyan, V. Ramanathan and B. K. Mishra, *J. Phys. Chem. A*, 2013, **117**, 6687–6694.

33 (*a*) V. I. Bakhmutov, *Dihydrogen Bond: Principles, Experiments, and Applications*, John Wiley & Sons, Inc., Hoboken, New Jersey, 2008; (*b*) J. Echeverria, G. Aullon, D. Danovich, S. Shaik and S. Alvarez, *Nat. Chem.*, 2011, **3**, 323–330.

34 (*a*) J. P. M. Lommerse, A. J. Stone, R. Taylor and F. H. Allen, *J. Am. Chem. Soc.*, 1996, **118**, 3108–3116; (*b*) M. Daszkiewicz, *CrystEngComm*, 2013, **15**, 10427–10430.

35 P. R. Spackman, M. J. Turner, J. J. McKinnon, S. K. Wolff, D. J. Grimwood, D. Jayatilaka and M. A. Spackman, *J. Appl. Crystallogr.*, 2021, **54**, 1006–1011.

36 H. Koga, A. Itoh, S. Murayama, S. Suzue and T. Irikura, *J. Med. Chem.*, 1980, **23**, 1358–1363.

37 SAINT V 7.34, *Software for the Integration of CCD Detector System, Bruker Analytical X-Ray Systems*, Madison, WI, 2008.

38 SADABS, V2008/2 and R. H. Blessing, Program for absorption corrections using Bruker-AXS CCD based on the method of Robert Blessing, *Acta Crystallogr., Sect. A:Found. Crystallogr.*, 1995, **51**, 33–38.

39 G. M. Sheldrick, *SHELXS-97, Program for Solution of Crystal Structures*, University of Gottingen, Germany, 1997.
40 G. M. Sheldrick, *SHELXL-97, Program for Refinement of Crystal Structures*, University of Gottingen, Germany, 1997.
41 DIAMOND, Crystal and Molecular Structure Visualization, *Crystal Impact GbR*, Bonn, 2016.
42 (*a*) F. Neese, *Wiley Interdiscip. Rev.: Comput. Mol. Sci.*, 2012, **2**(1), 73–78; (*b*) F. Neese, *Wiley Interdiscip. Rev.: Comput. Mol. Sci.*, 2022, **12**, e1606.
43 (*a*) C. Lee, W. Yang and R. G. Parr, *Phys. Rev. B: Condens. Matter Mater. Phys.*, 1988, **37**, 785–789; (*b*) A. D. Becke, *J. Chem. Phys.*, 1993, **98**, 5648–5652; (*c*) P. J. Stephens, F. J. Devlin, C. F. Chabalowski and M. J. Frisch, *J. Phys. Chem.*, 1994, **98**, 11623–11627; (*d*) E. Caldeweyher, S. Ehlert, A. Hansen, H. Neugebauer, S. Spicher, C. Bannwarth and S. Grimme, *J. Chem. Phys.*, 2019, **150**, 154122; (*e*) F. Weigend and R. Ahlrichs, *Phys. Chem. Chem. Phys.*, 2005, **7**, 3297–3305.
44 H. Kruse and S. Grimme, *J. Chem. Phys.*, 2012, **136**, 154101.
45 (*a*) CCDC 843028: Experimental Crystal Structure Determination, 2025, DOI: **10.5517/ccdc.csd.ccx97gw**; (*b*) CCDC 853691: Experimental Crystal Structure Determination, 2025, DOI: **10.5517/ccdc.csd.ccxnbf9**; (*c*) CCDC 864291: Experimental Crystal Structure Determination, 2025, DOI: **10.5517/ccdc.csd.ccy0ccn**; (*d*) CCDC 873772: Experimental Crystal Structure Determination, 2025, DOI: **10.5517/ccdc.csd.ccyb76p**; (*e*) CCDC 894172: Experimental Crystal Structure Determination, 2025, DOI: **10.5517/ccdc.csd.ccz0g8p**; (*f*) CCDC 929723: Experimental Crystal Structure Determination, 2025, DOI: **10.5517/ccdc.csd.cc106g2r**; (*g*) CCDC 929745: Experimental Crystal Structure Determination, 2025, DOI: **10.5517/ccdc.csd.cc106gsg**; (*h*) CCDC 929847: Experimental Crystal Structure Determination, 2025, DOI: **10.5517/ccdc.csd.cc106l2w**; (*i*) CCDC 963789: Experimental Crystal Structure Determination, 2025, DOI: **10.5517/ccdc.csd.cc11bwz7**; (*j*) CCDC 1432074: Experimental Crystal Structure Determination, 2025, DOI: **10.5517/ccdc.csd.cc1k25yr**; (*k*) CCDC 1447133: Experimental Crystal Structure Determination, 2025, DOI: **10.5517/ccdc.csd.cc1kkvqp**.